Preferential solvation dynamics in liquids: How geodesic pathways through the potential energy landscape reveal mechanistic details about solute relaxation in liquids

ARTICLE *in* THE JOURNAL OF CHEMICAL PHYSICS · SEPTEMBER 2010

Impact Factor: 2.95 · DOI: 10.1063/1.3481655 · Source: PubMed

2 AUTHORS:

Crystal Nguyen
University of California, San Diego
9 PUBLICATIONS **90** CITATIONS
SEE PROFILE

Richard M. Stratt
Brown University
122 PUBLICATIONS **4,279** CITATIONS
SEE PROFILE

Preferential solvation dynamics in liquids: How geodesic pathways through the potential energy landscape reveal mechanistic details about solute relaxation in liquids

Crystal N. Nguyen and Richard M. Stratt[a)]
Department of Chemistry, Brown University, Providence, Rhode Island 02912, USA

(Received 28 May 2010; accepted 2 August 2010; published online 24 September 2010)

It is not obvious that many-body phenomena as collective as solute energy relaxation in liquid solution should ever have identifiable molecular mechanisms, at least not in the sense of the well-defined sequence of molecular events one often attributes to chemical reactions. What can define such mechanisms, though, are the most efficient relaxation paths that solutions take through their potential energy landscapes. When liquid dynamics is dominated by slow diffusive processes, there are mathematically precise and computationally accessible routes to searching for such paths. We apply this observation to the dynamics of preferential solvation, the relaxation around a newly excited solute by a solvent composed of different components with different solvating abilities. The slow solvation seen experimentally in these mixtures stems from the dual needs to compress the solvent and to do solvent-solvent exchanges near the solute. By studying the geodesic (most efficient) paths for this combined process in a simple atomic liquid mixture, we show that the mechanism for preferential solvation features a reasonably sharp onset for slow diffusion, and that this diffusion involves a sequential, rather than concerted, series of solvent exchanges. © *2010 American Institute of Physics*. [doi:10.1063/1.3481655]

I. INTRODUCTION

Analyzing dynamics in terms of the kinds of excursions that are feasible on a potential energy landscape has proven very rewarding for certain kinds of problems, especially those with rugged energy landscapes.[1] Looking at the molecular motions responsible for the diffusion of fragile supercooled liquids, for example, told us that the increasing circuitousness of even the most efficient (*geodesic*) pathways through the landscape is connected quite directly with the orders-of-magnitude slowdown seen on lowering the temperature.[2,3] But does this kind of global examination of the potential energy landscape of the liquid say anything anywhere near as useful about more localized events, such as the critical elementary steps involved in chemical reaction dynamics in solution?

Solvation is a classic example of such an event.[4] It is a manifestly local process because it deals only with those solvent molecules that affect the potential energy of an individual solute molecule, but it can nonetheless be somewhat collective. The subpicosecond ("inertial") dynamics of even simple polar solvents such as acetonitrile[5] seems to involve the motion of the entire first solvation shell (a dozen or so molecules), and the subsequent diffusive dynamics is more collective still.[6] However, the collectivity of the process does not necessarily show itself in the overall dynamics that results. Typical dipolar and nondipolar laboratory solvents, such as acetonitrile and benzene, both tend to accomplish a substantial fraction of their solvation within a picosecond or two.[7–9] More viscous solvents such as ethylene glycol do exhibit a much slower solvation,[10] but that is largely because the final equilibration is a prisoner of the slow diffusion constants characteristic of these solvents.

Still, there is an interesting intermediate category of solvation in which the participating solvent molecules themselves are not intrinsically slow, but the net solvation process is much slower than one would expect from the properties of the individual contributing species. In *preferential solvation*, the solvation takes place in a mixture of solvents of different solvating abilities.[11] A slowdown then occurs solely because of the collective solvent rearrangement needed for the mixture to accommodate the differing solvation preferences of the various components.[12]

One way to think about such systems is to note that the presence of a second solvent component offers the system an additional relaxation pathway. In single-component solvents, ultrafast solvation is largely governed by the dynamics of the first solvation shell, and, in particular, in dipolar solvents, by first shell librational motions.[6] There is also a certain amount of net translation of solvent molecules into the first shell following any increase in the solute's charge or dipole moment ("electrostriction"). However, solvent mixtures have an extra translational option because of the possibility of replacing one kind of solvent in the first shell with another ("redistribution").[13–15] It is worth noting that despite the fact that this option is always available in a solvent mixture, not every mixture will exhibit the sharp dependence of solvation rate on solvent composition that we are concerned with here.[15–17] What seems to be needed in order to see a significant long-time component to the solvation is for the two translational modes to act in opposition with one another, thereby frustrating the solvation process.[9,18–21]

[a)]Electronic mail: richard_stratt@brown.edu.

That some kind of translational diffusion process lies at the heart of slow preferential solvation is now widely accepted.[8,9,12,14,22,23] Still, the mechanistic details of how this frustrated diffusion occurs, and why it leads to the slowing down it does, are much murkier. The mechanistic studies that have been carried out have noticed a high level of coordination between solvents leaving and entering the first solvation shell,[14,24,25] but constrained as they are to focusing on the immediate environs of the solute, they have not been in much of a position to comment on whatever collective, global rearrangements the solvent has to do in order to facilitate this coordination. To take this next step, what is clearly needed is a more system-wide picture of the entire solvation process.

In this paper we consider how a potential energy landscape perspective can allow us to not only look at, but quantify the collective character of this kind of solute relaxation process. To accomplish this task we proceed as follows. First, we show by carrying out molecular dynamics simulations that a remarkably simple model system for studying preferential solvation introduced by Sakurai and Yoshimori,[20] a single atomic solute dissolved in a binary mixture of atomic liquids, has most of the phenomenology we want to explore. One of the most striking results from the experimental studies of preferential solvation is that the solvation in a relatively slowly solvating solvent is hindered even further by mixing in a small fraction of a more rapidly solvating solvent.[8,23,26,27] We show that the model system reproduces this effect in a fairly dramatic fashion. Moreover, this model provides a nice vehicle for understanding how the conflicting requirements of solvent compression about an excited solute and solvent rearrangement about the solute tend to slow the solvation process.

Having established the relevance of this model system to more realistic experimental situations, we then apply our landscape analysis to this system by computing the different geodesic pathways responsible for successively more complete amounts of solvation. Interrogating these pathways gives us a count of the number of solvent atoms participating at each stage of the process. This number, in turn, allows us to make quantitative statements about the molecular mechanisms involved. In particular, even though our model lacks long-range electrostatic forces, we find preferential solvation to be a noticeably more sequential process than its single-solvent analog.

The remainder of the paper will be organized as follows. Section II summarizes both our molecular model and the numerical methods we use to perform molecular dynamics simulations and then uses these to present the basic dynamical features of preferential solvation–which are nicely captured by this model. Section III describes how we find the geodesics corresponding to solvation pathways. Section IV takes this information and shows how it can be used to reveal, in mechanistic detail, how preferential solvation differs from single-component solvation. We conclude in Sec. V with some general observations.

TABLE I. Potential energy parameters (Lennard-Jones well depths $\varepsilon_{\alpha\beta}$ between species α and β).

	Atom-atom pair[a]		
	v-v	u-S	u-W
Ground-state solute	ε	ε	ε
Excited-state solute	ε	3.0ε	1.5ε

[a]u refers to the solute, v to all solvents, S to strong solvents, and W to weak solvents.

II. OUR MODEL AND ITS BASIC DYNAMICS

A. Model and simulation protocols

There have already been a number of theoretical studies of solvation in solvent mixtures with fairly realistic depictions of the solvents and solutes used in typical experiments.[19,22] If our goal had been simply to carry out a new molecular dynamics simulation of such systems, it would not have been difficult to adopt one of these models for our purposes here. However, not only is it much more straightforward to carry out our geodesic pathway analysis in an atomic liquid, it turns out that an appropriately chosen mixture of an atomic solute and two different atomic solvents is sufficient to capture the full range of dynamical behavior we would like to understand.

The specific model, which was proposed and investigated by Sakurai and Yoshimori,[20] consists of N_s "strong" solvents (S), N_w "weak" solvents (W), and a single solute (u) capable of being in either a ground (g) or excited (e) electronic state, all interacting by Lennard-Jones pair potentials,

$$u_{\alpha\beta}(r) = 4\varepsilon_{\alpha\beta}[(\sigma/r)^{12} - (\sigma/r)^6], \quad (\alpha,\beta = \text{u-g,u-e,S,W}). \tag{2.1}$$

All of the species have the same mass m and diameter σ. Indeed, the potential parameters chosen (shown in Table I) have the two solvents differing only in how strongly they interact with the solute in its excited-state. That is, the three solvent-solvent well depths are taken to be identical, $\varepsilon_{SS} = \varepsilon_{WW} = \varepsilon_{SW}$, with no dependence on the solute state, and those, in turn, are made identical to the two solvent/ground-state-solute well depths, $\varepsilon_{u\text{-}g,S} = \varepsilon_{u\text{-}g,W} = \varepsilon_{SS}$. By contrast, the two solvent/excited-state-solute well depths differ both from each other and from the corresponding ground-state well depths. Consistent with the commonly observed behavior of eximeric systems, both solvents are assumed to interact more strongly with the excited-state solute than with its ground-state counterpart, but this effect is made even more prominent in the strong solvents, causing the excited solute to have a significant preference for having strong solvents in its first solvation shell.[28]

We confine ourselves to a single liquid-phase thermodynamic state, a reduced density ρ, and reduced temperature T of

$$\rho\sigma^3 = 0.80, \quad k_B T/\varepsilon = 1.00 \pm 0.03,$$

with ε is the reference (solvent-solvent) well depth and k_B is Boltzmann's constant. Except where explicitly noted, all of our calculations are carried out with a total of 256 atoms

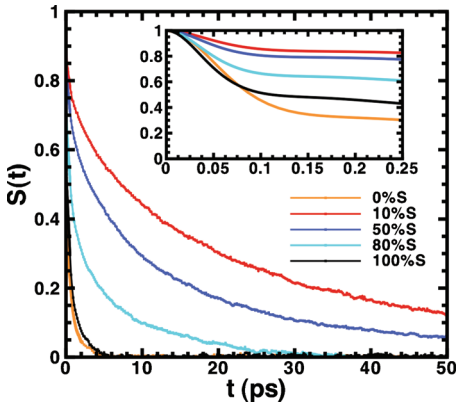

FIG. 1. The dependence of solvation dynamics on the solvent composition for the model used in this paper. The nonequilibrium solvation response function S(t) is shown for solutions consisting of 0%, 10%, 50%, 80%, and 100% S solvents. The larger scale figure depicts the longer-time-scale diffusive relaxation; the insert shows the initial (subpicosecond) inertial relaxation for the same solutions.

(one solute and $N_S+N_W=255$ solvent atoms), although to assess the scaling with system size, we also perform a study with a total of 500 atoms (one solute and $N_S+N_W=499$ solvent atoms). To help us calibrate the relevant time scales, we report all of our numerical values of time using the standard Ar choices for the solvent ε, σ, and m parameters [which sets the Lennard-Jones time scale $\tau_{LJ}=(m\sigma^2/\varepsilon)^{1/2}=2.16$ ps].[29]

Molecular dynamics simulations were implemented using the velocity Verlet algorithm with a time step $\delta t=2.5\times10^{-3}$ $\tau_{LJ}=5.4$ fs, and cubic periodic boundary conditions.[29] Equilibrated ground-state liquid configurations were achieved by melting a fcc lattice with a random distribution of the three components, repeatedly rescaling the kinetic energy to obtain the desired temperature, and then allowing the system to relax for $1.1\times10^6\delta t=5.9$ ns. When needed, equilibrated excited-state liquid configurations were found from their equilibrated ground-state counterparts by instantaneously changing the solute-solvent potentials and then repeating the ground-state rescaling and equilibration protocols. All of the molecular dynamics results presented here, except those for the radial distribution functions and those for the pure weak solvent, are averages over 12 000 initial configurations (generated by sampling our trajectories every $10\delta t$). Results for the pure weak solvent are averaged over 300 000 configurations. Radial distribution functions are averaged over 10^6 configurations.

B. Molecular dynamics results

The essential features of preferential solvation in this system are amply illustrated by the distinct nonequilibrium responses seen with different solvent mixtures, Fig. 1. In each case, an equilibrated ground-state solute/solvent mixture is instantaneously perturbed by exciting the solute to its excited-state. The traditional solvation response function

$$S(t)=\frac{\overline{\Delta V_{uv}(t)}-\overline{\Delta V_{uv}(\infty)}}{\overline{\Delta V_{uv}(0)}-\overline{\Delta V_{uv}(\infty)}}, \tag{2.2}$$

with $\Delta V_{uv}(t)$ as the excited-state/ground-state energy gap (the difference between e and g solute-solvent potential energies) evaluated at a time t after the excitation, and the overbars indicating a nonequilibrium average over the $t=0^-$ initial conditions, then provides a normalized measure of the extent of the energy relaxation that has yet to occur.

Both the pure strong solvent case and the pure weak solvent case show the kind of ultrafast relaxation that one has come to expect with small organic solvents.[4] In fact, despite the twofold difference in excited-state interaction strengths, the two solvents follow virtually identical relaxation profiles for the first few picoseconds. [It is worth noting how surprising the lack of difference between the two solvents is. Although one can think of this comparison as being mathematically equivalent to contrasting two different (excited-state) solutes dissolved in the same solvent, and although an invariance to switching solutes is commonly associated with linear response theory, linear response behavior *per se* requires no such *solute independence*. It requires only that the relaxation to equilibrium for a given Hamiltonian be the same as the decay of the fluctuations about equilibrium for that same Hamiltonian. There is no requirement that relaxations governed by different Hamiltonians should follow the same dynamics.][30] However, when these two solvents are mixed, the dynamics slows markedly. Somewhat counterintuitively, we obtain the very slowest relaxation when we take the least driven nonequilibrium situation, the one with 100% weak solvent, and we begin to *increase* the driving force by replacing 10% of the weak solvent by strong solvent.[31]

This same basic pattern is precisely what shows up in time-dependent-fluorescence experiments with mixed solvents such as acetonitrile and benzene.[8,9] Unlike our simple model, pure dipolar solvent acetonitrile and the pure nondipolar solvent benzene do not have identical ultrafast relaxation profiles; with a typical coumarin solute, the former completes 80% of its relaxation within 300 fs,[5] whereas the latter takes about 2 ps. However mixing these solvents slows the relaxation even more, with the very slowest relaxation occurring when 5% of the (presumably) slower solvent benzene has been replaced by the (presumably) faster solvent acetonitrile.

The essential origins of the slowdown, as we noted in the Introduction, lie in the gross solvent rearrangements needed to turn equilibrated ground-state liquid configurations into the configurations preferred by the excited-state. With our model system it is easy to get an overview of this process by watching the time evolution of the radial distribution functions for each solvent component (Fig. 2), noting, in particular, the evolving populations of strong and weak solvents in the first solvation shell (Fig. 3).

With 10% strong solvent, for example, the equilibrium first-solvation-shell arrangement around the ground-state solute contains, on the average, about 1.3 S and 11 W solvent molecules. The excited-state, by contrast, has an average of 2.8 S and 10 W solvents. A sizeable fraction of the slow dynamics is thus caused by the need for one to two extra

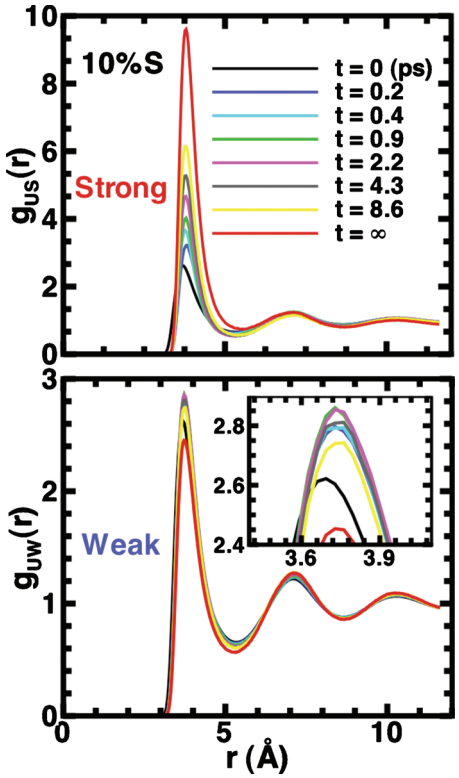

FIG. 2. The time evolution of solvent structure around the excited-state solute for the 10% S case. What we plot here are both the solute/strong solvent radial distribution function $g_{uS} \equiv g_{u\text{-}e,S}(r;t)$ and the solute/weak solvent radial distribution function $g_{uW} \equiv g_{u\text{-}e,W}(r;t)$ following a $t=0$ excitation of the solute from the ground to the excited-state. The insert in the lower panel highlights the nonmonotonic weak solvent behavior seen in the first shell peak: although the peak height eventually ends up being smaller than its initial value, during the initial (solvent compression) phase, this height actually grows. It is not until after the first 1–2 ps that the peak height begins to shrink.

S molecules to force their way through a dense medium into the first solvation shell, for those molecules to expel a W molecule, and for that W to meander into the bulk liquid. This slow *solvent switching* process is evidenced most dramatically by the growth of the first peak of the uS (solute/strong solvent) radial distribution function. However, as we can see from the net growth of the total first shell population,

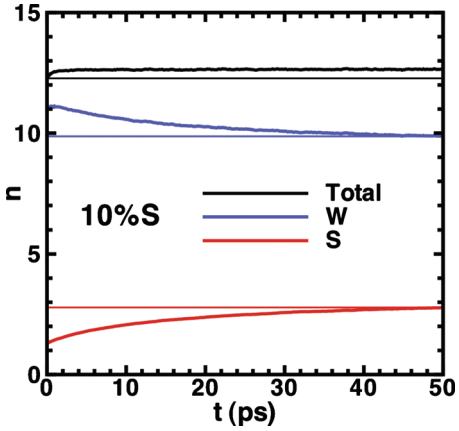

FIG. 3. The time evolution of the first solvation shell population for the 10% S case. The curves drawn here are derived by integrating the radial distributions functions shown in Fig. 2 to the first minimum.

from 12.3 to 12.8 molecules, what also has to be playing a role is the net *solvent compression* about the first shell on solute excitation (what one would have called "electrostriction" with more commonplace dipolar solutes). The compression occurs because both the weak and the strong species are more strongly attracted to the excited-state solute than they are to the ground-state. This same enhanced attraction, though, means that in spite of the energetic favorability of trading a weak solvent for a strong one, it is energetically uphill for a weak solvent to depart in the absence of such a coordinated solvent switch. The solvent compression can therefore be thought of as actively frustrating the solvent switching process.

Part of what makes this frustration so effective in slowing the overall solvation is that the timing of these events could not be worse. Figure 3 makes it clear that the compression builds up well before any switching can take place: the e^{-1} time for the growth of the total number of first-solvation-shell solvents is 0.7 ps, far less than the comparable e^{-1} relaxation times for the first-solvation-shell populations of the individual S (12 ps) and W (15 ps) solvents. Interestingly, this is precisely what one sees with more realistic solvents. Ladanyi and Perng[9] noted that acetonitrile/benzene mixtures also exhibit a fast electrostriction event followed by slow solvent redistribution.

That the end result of the entire solvation process is just the net transport of a few molecules, then, is a bit deceptive. In a dense liquid there has to be some level of cooperativity for even a modest solvent reorganization to occur. We turn next to seeing how much we can learn about this many-body cooperativity from the geometry of the associated potential energy landscape.

III. DETERMINING THE MOST EFFICIENT SOLVATION PATHWAYS

A. Geodesic pathways in the potential energy landscape ensemble

It is not at all obvious that there should be dynamically optimum pathways defined by the potential energy landscapes of liquids. Indeed, the idea that there should be some purely geometrically prescribed optimal route through the many-body configuration space, independently of such kinematic features as molecular speed, is a bit surprising. However, for at least some dynamical problems, there are such routes, and as we emphasized in our previous work,[3] one can find them by looking solely at the geometry of the potential energy surface.

For the diffusion of an N-atom atomic liquid, for example, we showed that the relevant paths are the geodesic (shortest) paths that the 3N atomic coordinates $\mathbf{R} = \{\mathbf{r}_1, \ldots, \mathbf{r}_N\}$ can take − and that the lengths of these paths can be used to predict the diffusion constants.[3] However, even for this simple a problem, defining precisely what one should mean by "shortest" needs a certain amount of care. At a finite temperature, the rigorously shortest pathway is always the trivial straight line connecting the end points; it is formally irrelevant that such a line would have to pass through unphysically high-lying regions of the potential sur-

face because a Boltzmann factor always allows *some* probability of the system being located at any **R**. The physical geodesic, though, comes from asking for the shortest path lying within the *potential energy landscape ensemble* associated with that temperature.[2] That is, for each temperature T, we need to constrain the pathways to include only those configurations **R** whose potential energy $V(\mathbf{R})$ never rises above what we call the landscape energy E_L for that T,

$$V(\mathbf{R}) \leq E_L(T). \tag{3.1}$$

One can show that for this ensemble, all of the allowed **R** are equally probable, and that for there to be thermodynamic equivalence between this ensemble and the canonical ensembles, $E_L(T)$ must be numerically equal to $\langle V \rangle$, the canonical ensemble average potential energy at temperature T.[2] So, it is clear how to sample from this ensemble within a simulation, at least in the thermodynamic limit.

The landscape-energy-dependent lengths of the geodesics computed in this fashion have proven to be accurate predictors of the strongly temperature-dependent diffusion[3] seen in the Kob–Andersen model for supercooled liquids,[32] a binary atomic mixture. We therefore might expect our analysis to fare equally well when applied to the more prosaic binary atomic mixture model being considered in this paper. However there is an important distinction between the global transport problem presented by bulk diffusion and the local relaxation problem we are facing here. To see this point, it is useful to place both of these problems in context.

By analogy with the more standard treatments of liquid-state dynamics, one could imagine looking for either nonequilibrium or equilibrium geodesic pathways. For example, we could determine our starting configurations by choosing a set of initial configurations appropriate for the relevant nonequilibrium experiment. That would mean having macroscopic density inhomogeneities in the case of bulk diffusion and some kind of microscopically out-of-equilibrium solvent arrangement in the case of solvation dynamics. Alternatively, and more simply, one could just pick the initial and final configurations from the equilibrium ensemble (in effect, adopting the linear response perspective of deriving the desired dynamics from the equilibrium fluctuations).

The end points needed for bulk diffusion geodesics are easy to find within this latter equilibrium approach, as our earlier work has shown.[3] Given an equilibrium set of initial configuration $\mathbf{R}_i$, one can obtain an equilibrium set of matching final configurations, $\mathbf{R}_f$, by conventional Monte Carlo methods, adding only the constraint that the 3N-dimensional end-to-end distance between the configurations,

$$\Delta R \equiv |\mathbf{R}_f - \mathbf{R}_i|, \tag{3.2}$$

has some desired value.

In a solvation problem, though, the preeminent role of a single molecule (the solute) means an equilibrium sampling of the entire solution would hopelessly under-represent the key local fluctuations in the vicinity of that special molecule's location. We must therefore come up with a nonequilibrium generalization of our previous work more suitable for studying local relaxation. We can do so by first recognizing that S(t), the solvation response function itself, Eq. (2.2), acts as a many-body coordinate useful for focusing on precisely the important regions of configuration space.[33] The desired final configurations should therefore be found by constraining our Monte Carlo sampling to achieve predetermined values of both ΔR and $s = S(t_{final})$.

$$s = \frac{\Delta V_{uv}(\mathbf{R}_f) - \langle \Delta V_{uv} \rangle_e}{\Delta V_{uv}(\mathbf{R}_i) - \langle \Delta V_{uv} \rangle_e}. \tag{3.3}$$

Still, to make the geodesics genuinely representative of an actual solvation experiment (such as a time-dependent fluorescence measurement), we need to add yet other requirements to ensure that the initial and final configurations, and the pathway between them, are consistent with what one would see in such an experiment. In this experiment one starts with a solvent arrangement in equilibrium with the solute in its electronic ground-state, but watches the solution evolve under the influence of the potential surface determined by the electronically excited solute. That means while $\mathbf{R}_i$ has to be selected from the ground-state equilibrium distribution, the average solute energy gap $\langle \Delta V_{uv} \rangle_e$ is set by the equilibrium excited-state solute distribution. More than that, if we really want the s value for a pathway to measure its fractional progress toward equilibration, the pathway's final configuration, $\mathbf{R}_f$ should correspond to a distance ΔR consistent with the mean-first-passage time needed to achieve that value of s. Without this last stricture, almost all of the final liquid configurations one would sample would differ only in their placements of far-from-the-solute-solvent molecules.

TABLE II. Thermodynamics properties of solutions with an excited solute. [For each of the excited-state-solute/solvent mixtures studied in this paper, we give the temperature T, landscape energy $E_L^{(e)}$, and average solute energy gap $\langle \Delta V_{uv} \rangle_e$, all reported in units of the reference well depth ε. The mixtures with a ground-state solute all have $k_BT/\varepsilon = 1.00$, $E_L^{(g)}/(N\varepsilon) = -5.362$, and $\langle \Delta V_{uv} \rangle_g/\varepsilon = -6.89 \pm 1.49$ (independently of the solvent composition). To help calibrate the differences in the solvation thermodynamics, we also report the equilibrium Stokes shift $\Delta E = \langle \Delta V_{uv} \rangle_e - \langle \Delta V_{uv} \rangle_g$ for each mixture.]

	Mixture composition (% S)			
	10	50	80	100
(N_S, N_W)[a]	(26, 229)	(127, 128)	(204, 51)	(255, 0)
k_BT/ε	1.005	1.004	1.004	1.006
$E_L^{(e)}/(N\varepsilon)$	−5.404	−5.442	−5.461	−5.466
$\langle \Delta V_{uv} \rangle_e/\varepsilon$	-9.93 ± 1.91	-19.36 ± 2.30	-23.30 ± 1.94	-25.53 ± 1.63
$\Delta E/\varepsilon$	−3.04	−12.47	−16.41	−18.64

[a]Actual numbers of strong (S) and weak (W) solvent atoms comprising the indicated N=256-atom solvent-plus-solute mixtures.

B. Computational approaches

We began by using a molecular dynamics calculation to determine the average solution potential energies, and thus the proper landscape energies $E_L^{(e)}$, for our equilibrated excited-state-solute solutions. The results (Table II) show that, as one might expect with a fixed target temperature, $E_L^{(e)}$ is fairly constant over a wide range of solution compositions, even though the final Stokes shifts,

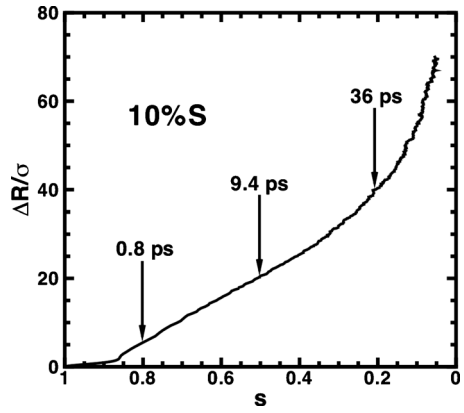

FIG. 4. Relationship between the average net configuration space (3N-dimensional) distance traveled and the average extent of solvation accomplished for the 10% S case. Both the average net distance $\Delta R(t)$ (plotted in units of σ) and the average solvation progress measure $s=S(t)$ depend parametrically on the elapsed time t; the graph shown combines the two averages to determine their time-independent relation.

$$\Delta E = \langle \Delta V_{uv} \rangle_e - \langle \Delta V_{uv} \rangle_g, \tag{3.4}$$

the differences between the excited- and ground-state-equilibrated energy gaps, vary by more than a factor of 6. All the averages reported for this calculation are over 10^6 liquid configurations. Molecular dynamics simulations were also used to determine the average relationship between 3N-dimensional distance traveled during solvation ΔR, and the final value of the solvation response function S(t). This information was deduced by computing the non-equilibrium averages S(t), Eq. (2.2), and $\Delta R(t)$,

$$\Delta R(t) = \overline{|\mathbf{R}(t) - \mathbf{R}(0)|}, \tag{3.5}$$

allowing us to identify the aforementioned mean-first-passage distance for a given value of $s=S(t)$ as $\Delta R(s) \equiv \Delta R(t(S))$. The resulting dependence of ΔR on s is shown in Fig. 4 (with nonequilibrium averages based on 6000 initial phase-space points).

With these preliminaries out of the way, trial initial configurations for our pathways $\mathbf{R}_i$ were selected by performing a potential energy landscape ensemble Monte Carlo sampling of the liquid with a ground-state solute.[34] If on promoting this configuration into the excited-state, the configuration was found to be a member of the excited-state potential energy landscape ensemble [that is, if $V^{(e)}(\mathbf{R}_i) \leq E_L^{(e)}$], that liquid geometry was then taken as the starting point for a pathway. If not, the configuration was moved along the 3N-dimensional gradient of the excited-state potential and the next step along the pathway $\mathbf{R}_i'$ was identified as the first new configuration found satisfying $V^{(e)}(\mathbf{R}_i') \leq E_L^{(e)}$. Pathway end points $\mathbf{R}_f$ were then located by performing a landscape ensemble Monte Carlo sampling of the excited-state potential surface, starting from each $\mathbf{R}_i'$.[34] The final $\mathbf{R}_f$ were defined to be the first liquid configurations having both the desired value of s (within ± 0.01) and the expected associated value of $\Delta R = \Delta R_s$ (to within a tolerance of 0.1σ for binary mixtures and 0.01σ for pure solvents).

Given 120 such ($\mathbf{R}_i$ and $\mathbf{R}_f$) end point pairs, candidate $\mathbf{R}_i \rightarrow \mathbf{R}_f$ geodesic pathways in the excited-state potential surface were constructed by using the approach derived in our earlier work.[3] The system is moved with trial steps of 0.001σ in the precise direction of $\mathbf{R}_f$, translating along the 3N-dimensional gradient of the potential whenever necessary to escape energetically forbidden ($V^{(e)}(\mathbf{R}) > E_L^{(e)}$) configurations.

As we showed when we worked out the foundations of our landscape geodesic analysis, paths obtained in this simple fashion automatically fall into the class of rigorously optimum solutions to our most efficient path problem.[3] However we also noted that this algorithm is not guaranteed to (and, in general, will not) produce the single most efficient path. To obtain the final paths, we therefore took the candidate paths produced by this algorithm and subjected them to the same kinds of local refinements that we found to be useful in our studies of liquid diffusion.[35] All of the results reported in this paper make use of averages over such optimized paths (though there were no significant qualitative differences that we ever saw between the optimized and unoptimized pathways).

IV. DETERMINING MECHANISTIC INFORMATION

A. Lengths of geodesic pathways

We noted in our earlier work that the values of macroscopic diffusion constants were governed by how much longer the geodesic pathways were than the direct end-to-end distance being traversed. Defining g to be the geodesic path length and ΔR to be the net distance covered in configuration space, we found, in particular, that

$$D/D_0 = \lim_{\Delta R \rightarrow \infty} (\Delta R/g)^2$$

(with D_0 the high-temperature reference value for the diffusion constant needed to incorporate the few-body kinematics), so the slowest diffusion occurs when the ratio $(g/\Delta R)$ begins to be significantly larger than 1.[3]

Here, we are interested not in finding the diffusion constant of our bulk solvent, but in how the solvent's inertial motion around the solute turns into slow diffusion. It is therefore informative to watch how the geodesic path length changes as our solvation process proceeds, Fig. 5. Each point in the graph reports the average value of the "conductivity" ratio $(\Delta R/g)^2$ as a function of the solvation response measure s, Eq. (3.3), for the geodesic paths. In a sense, s measures the fraction of solvation that the path has yet to accomplish, so the smaller the value of s, the closer a path is to achieving equilibration.

For a single-component S solvent, the conductivity ratio stays close to 1 as s drops from 1.0 to 0.1, indicating that ordinary solvation is not especially diffusive over the roughly 1.6 ps that it takes this system to carry out its first decade of solvation. As more weak solvent is added, however, the conductivity ratio begins to drop from 1, and to do so at progressively earlier stages in the solvation. For solvents with 80%, 50%, and 10% S species, the departure from largely inertial solvation seems to begin at $s=0.3$, 0.6, and 0.7, respectively. Curiously, each of these events takes about the same amount of physical time (1.6 ± 0.2 ps), but the high s values at which these last two mixed solvents lose their inertial character means that a significant fraction of the

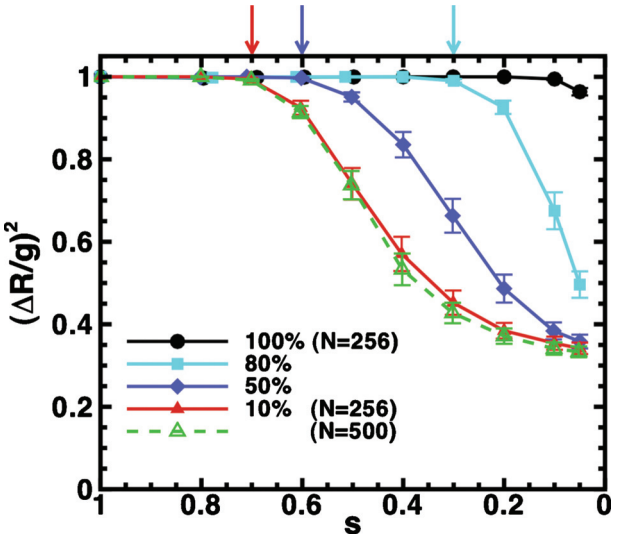

FIG. 5. The growth of the most efficient (geodesic) path length during preferential solvation. Unlike the earlier figures, which reported molecular dynamics, this figure looks solely at the geometry of the solution potential energy landscape. A set of geodesic paths is found, and the average conductivity ratios (the square of the direct-to-geodesic-path-lengths quotient, $(\Delta R/g)^2$) are shown as a function of average solvation progress, s, for 10%, 50%, 80%, and 100% S solvents. (In addition, for the 10% S case, we plot the results for both N=256 atom and N=500 atom solutions, demonstrating that finite size effects are negligible.) The color-coded arrows drawn above the figure indicate the locations we identify (from left to right) as the onsets of diffusive pathways for the 10%, 50%, and 80% S solvents, respectively.

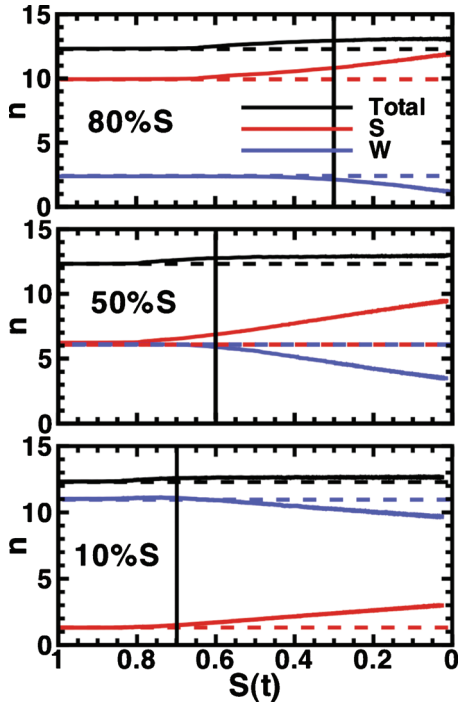

FIG. 6. The evolution of the first-solvation-shell populations plotted as a function of the solvation progress variable S(t) for the three solvents shown. The figure, which simply replots the kinds of molecular dynamics results portrayed in Figs. 1 and 3 on a single graph, emphasizes that the first shell numbers of strong solvent (S), weak solvent (W), and total solvent begin to exhibit noticeable changes at different points in the solvation process. Vertical lines, drawn at the same locations as the arrows in Fig. 5, indicate the points at which the geodesic analysis predicts that the dynamics is becoming strongly diffusive.

preferential solvation that will eventually occur needs to do so via a diffusive mechanism. With the 10% S solvent in particular, only 30% of the progress toward the full Stokes shift is accomplished by inertial means.

So what is different about the molecular motion in the mostly inertial and mostly diffusive parts of the pathways? A useful clue comes from re-examining the evolving composition of the first solvation shell, the kind of structural information given in Fig. 3, but as a function of the solvation response S(t) rather than elapsed time. When plotted in these terms, Fig. 6, we notice that the inertial-to-diffusive transitions always seem to coincide with the first significant expulsion of the weak solvent component. The subsequent non-neighboring-solvent rearrangement must therefore be an essential element of the slowest diffusion. The strong component by contrast, the one presumably more influenced by the onset of excited-state-solute forces, invariably begins entering the first shell at or before this stage in the solvation. The attending net growth in first shell population (the fast solvent compression) would thus seem to be basically an inertial effect.

B. The number of solvent atoms participating in the geodesic pathways

The lengths of the geodesic pathways are not the only information that we can extract from these paths. In principle, the pathways themselves describe a kind of idealized microscopic mechanism for our process in much the same way that inherent structures describe the essentials of molecular arrangements in liquids.[36] We should therefore be able to discern mechanistic details from the actual *sequence* of atomic locations found along the pathways.

One of the more interesting approaches to getting such information uses the actual number of solvent atoms with some level of significant participation along the path. To get at this number, suppose we begin by thinking about what defines the directions of our paths. There is no true dynamics with our paths (in the sense of a prescription for how our configurations evolve with physical time), but what we do have is a progress variable τ that tracks the sequence of atomic configurations $\mathbf{R}(\tau)$ from their initial $\mathbf{R}_i=\mathbf{R}(0)$ to their final $\mathbf{R}_f=\mathbf{R}(1)$ locations. It is thus natural to define a "velocity" by finite difference

$$\dot{\mathbf{R}}(\tau_a) \equiv (\mathbf{R}(\tau_{a+1}) - \mathbf{R}(\tau_{a-1}))/(\tau_{a+1} - \tau_{a-1}), \tag{4.1}$$

with a as an index labeling the discrete set of configurations constituting each path.

As with the individual configurations, the velocities can be thought of as 3(N−1)-dimensional vectors,

$$\dot{\mathbf{R}}(\tau) \equiv \sum_{j\mu} \dot{r}_{j\mu}(\tau)|j\mu\rangle \tag{4.2}$$

(with $j=1,\ldots,N-1$ labeling the N−1 solvent atoms and $\mu=x,y,z$ denoting the Cartesian directions), allowing us to specify the instantaneous directions of our paths by 3(N−1)-dimensional unit vectors with a normalized set of components $c_{j\mu}(\tau)$,

$$\hat{\mathbf{R}}(\tau) = \dot{\mathbf{R}}(\tau)/|\dot{\mathbf{R}}(\tau)| \equiv \sum_{j\mu} c_{j\mu}(\tau)|j\mu\rangle, \quad \left(\sum_{j\mu} c_{j\mu}^2(\tau) = 1\right). \tag{4.3}$$

For our purposes it is also useful to think about the (normalized) total contribution to a path's direction that we can attribute to each atom, $c_j(\tau)$,

$$c_j^2(\tau) \equiv \sum_{\mu} c_{j\mu}^2(\tau) = \sum_{\mu} \dot{r}_{j\mu}^2(\tau)/\sum_{j\mu} \dot{r}_{j\mu}^2(\tau), \tag{4.4}$$

$$\sum_{j=1}^{N-1} c_j^2(\tau) = 1. \tag{4.5}$$

However, this unit-vector language, Eq. (4.3), makes it look as if we have a quantum mechanical wave function described in Hilbert space. Hence, by analogy with what is often done in quantum studies of localization, we can define an instantaneous inverse participation ratio IPR(τ),[37]

$$\mathrm{IPR}(\tau) \equiv \sum_{j=1}^{N-1} c_j^4(\tau), \tag{4.6}$$

which acts as a measure the number of participating basis functions, or in our case, the number of participating atoms. The basic idea is that if it were true that only n out of the $N-1$ solvent atoms were displaced at some point along the geodesic path ($1 \le n \le N-1$), but those that were displaced had identical "velocities," then Eqs. (4.5) and (4.6) would tell us that

$$c_j(\tau) = 1/\sqrt{n} \quad (j = \text{any one of the n moving atoms}),$$

$$c_j(\tau) = 0 \quad (\text{otherwise}),$$

$$\mathrm{IPR}(\tau) = n(1/\sqrt{n})^4 = 1/n,$$

so that the reciprocal of the inverse participation ratio (the "participation ratio") would report exactly this n value. With less idealized situations there is no unique definition of such a number of participating atoms, but because the IPR describes the full range from complete localization of an excitation on a single atom to complete delocalization over the entire system, it is often taken as a reasonable measure of participation.

Our level of solvent participation presumably varies along our paths, but it is revealing to consider just the average participation number for each path taken as a whole

$$n = \langle \mathrm{IPR}^{-1} \rangle = \int_0^1 d\tau\, \mathrm{IPR}^{-1}(\tau). \tag{4.7}$$

One obvious question, then, would be how this n changes with the amount of solvation accomplished by different paths [as measured by their different s values, Eq. (3.3)]. However, we can probe a little more deeply. These average participation numbers depend strongly on the specifics of the initial and final configurations chosen for the path. What we really want to know, though, is what kinds of paths the potential energy landscape directs our system to take *between* the end points. We can extract this information by looking not at the n value itself, but how different this value is from the value for the direct path between the same end points, that is, how different the participation number is for the most efficient path the system could take with a perfectly flat landscape.

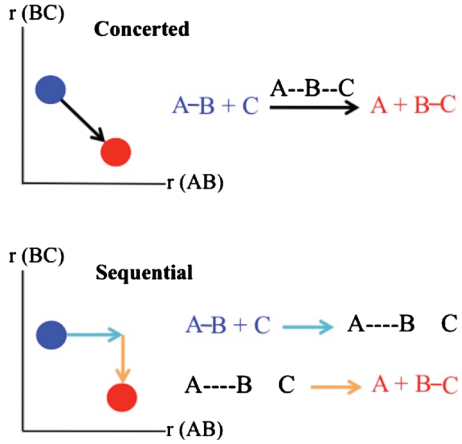

FIG. 7. Extracting mechanistic information from the number of degrees of freedom waiting to participate. Whether we would say that the hypothetical $A-B+C \rightarrow A+B-C$ chemical reaction illustrated here proceeds in a single concerted step, or as a sequence of two steps, depends on whether the shortening of the BC distance r(BC) takes place at the same time as (upper panel), or after (lower panel), the lengthening of the AB distance r(AB).

$$\Delta n = n^{\text{direct}} - n^{\text{actual path}}. \tag{4.8}$$

This difference provides us with a quantitative way of answering the classic mechanistic question of whether the mechanism followed by our process is concerted or sequential. Consider, by way of example, the quintessential one-dimensional chemical reaction portrayed in Fig. 7.

$$A - B + C \rightarrow A + B - C.$$

The differerence in bonding between reactants and products requires that, sometime before the final state is reached, the distance r(AB) needs to increase and the distance r(BC) needs to decrease. Thus, the number of coordinates involved in the net change, $n^{\text{direct}}=2$. If the reaction mechanism itself were concerted, both coordinates would have to move simultaneously, so this number would also be the number of coordinates involved in the real path. Hence,

$$\Delta n^{\text{concerted path}} = 2 - 2 = 0.$$

However, if the reaction took place in a sequential fashion, only one coordinate would be moving at a time, so the average number of coordinates moving at any stage along the path [as computed in Eq. (4.7)] $n^{\text{actual path}}=1$. Thus

$$\Delta n^{\text{sequential path}} = 2 - 1 = 1.$$

Hence by measuring the *number of atoms waiting to move* (or that have already moved), Δn reports on the molecular timing involved in the mechanism.

We plot this waiting-to-participate number in Fig. 8 for three of our preferential solvation examples. In each case it seems evident that the mechanism of the solvation explicitly shifts from a clearly concerted pathway ($\Delta n=0$) to one in which there is a distinct sequential character and that it does so precisely at the point we have identified as the inertial-to-

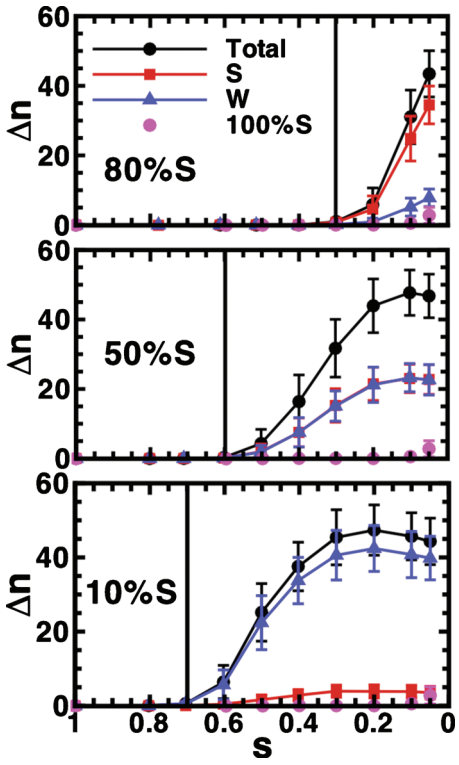

FIG. 8. The number of solvent atoms waiting to move, Δn, in preferential and ordinary solvation, as determined from the participation numbers associated with the landscape geodesics. The three panels present the waiting numbers of weak, strong, and total solvent atoms for the 10%, 50%, and 80% S solutions, each as a function of the solvation progress variable s. For comparison, each panel also shows (as dots practically indistinguishable from the horizontal axes) the results from the pure solvent (100% S) case. As in Fig. 6, we draw vertical lines where the growing lengths of the geodesic paths indicate that the dynamics is starting to become strongly diffusive.

diffusive transition. By contrast, for solvation in a pure solvent (which we also show for comparison), the waiting number $\Delta n=0$ throughout at least the first decade of the solvation. The slowing down associated with preferential solvation can thus be attributed, fairly unambiguously, to the need for solvent-solvent exchanges to occur *seriatim*, with each move awaiting its turn. Solvent compression (or electrostriction) has no such mechanistic requirements, making it hardly surprising that that process happens first.

V. CONCLUDING REMARKS

From a landscape perspective what is intriguing about preferential solvation is that it leads to slow dynamics even when there are no easily identifiable potential barriers that need to be surmounted. Slow preferential solvation is not specific to hydrogen bonding solvents or to the presence of strong electrostatic forces, for example. The dynamics is slow in our systems solely because of the intricate collective motion needed to reach equilibrium from the experimentally accessible starting configuration, or as we would put it here, because of the limited pathways available through the potential energy landscape with our initial conditions.

Examining those pathways proved to be rather revealing, especially in combination with our own and previous molecular dynamics studies of preferential solvation.[9,14,19,20,22,24,25,38] Mixed solvents suddenly confronted by an electronically excited solute seem to evolve two fundamentally separate ways. The first response is a net solvent compression around the solute. With typical laboratory solutes and solvents this compression arises from the electrostriction induced by the presence of an increased solute dipole.[9,14,15,18,24] But we see an equivalent effect here even without such forces. Within our model, the geodesic-path-length and geodesic-path participation number calculations tell us that this tendency to crowd around the solute is a simultaneous and largely inertial response of the local solvent.

In mixed solvents, however, there is a surprisingly well-defined point at which this driven dynamics is evidently replaced by a largely diffusive solvent motion. We see the geodesic pathways beginning to lengthen, signaling the onset of diffusion, and we can watch those same geodesics beginning to take on a significantly sequential character. It is worth noting that this nonconcertedness, in particular, is something that would have been difficult to quantify without having the geodesics at our disposal. Our mechanistic evidence came fundamentally from comparing the typical number of atoms participating at each point along a geodesic path with the net participation for the whole path. Had we tried to infer mechanisms by simply following the full molecular dynamics,[14,24,25] the presence of random solvent fluctuations (which we effectively removed by finding geodesic paths), would probably have obscured our key finding that there really are certain specific kinds of solvent motions that can be identified as the principal ingredients in the unusually slow solvation.

We do, of course, need to go back and ask how dependent our specific conclusions are on the idealized molecular models we studied. One might expect that the lack of reorientational degrees of freedom in our solvent might not be all that critical: the long-time dynamics is largely governed by translational diffusion into and out of the first solvation shell.[8,9,12,14,22,23] Still, coupling between translation and rotation in dense liquids could, in principle, influence the geodesic pathways. Similarly, while neither hydrogen bonding nor electrostatic forces between solvents seem to be prerequisites for slow preferential solvation,[22,24] they both could end up redirecting the most efficient pathways.[17] The presence of larger, more realistic, solutes could also have a noticeable quantitative effect.[9,17,19,22]

Nonetheless, even for the limited model we used here, it seems likely that a more detailed interrogation of the geodesic paths could lead to much more detailed pictures of liquid-state relaxation mechanisms. Looking at the identity of the participating atoms and the geometry of their optimum movements, for example, could easily paint a much richer portrait than one could ever get simply by counting those atoms; all one has to do is to figure out how best to extract that kind of information from the geodesics we already know how to find.

ACKNOWLEDGMENTS

We thank Dr. Chengju Wang for a number of helpful suggestions regarding the implementation of this landscape analysis. This work was supported by NSF Grant No. CHE-0809385.

[1] M. S. Shell, P. G. Debenedetti, and F. H. Stillinger, J. Phys. Chem. B **108**, 6772 (2004); B. Doliwa and A. Heuer, Phys. Rev. E **67**, 031506 (2003); D. J. Wales, *Energy Landscapes* (Cambridge University, Cambridge, 2003); J. N. Onuchic, Z. Luthey-Schulten, and P. G. Wolynes, Annu. Rev. Phys. Chem. **48**, 545 (1997).
[2] C. Wang and R. M. Stratt, J. Chem. Phys. **127**, 224503 (2007).
[3] C. Wang and R. M. Stratt, J. Chem. Phys. **127**, 224504 (2007).
[4] R. M. Stratt and M. Maroncelli, J. Phys. Chem. **100**, 12981 (1996).
[5] S. J. Rosenthal, X. Xie, M. Du, and G. R. Fleming, J. Chem. Phys. **95**, 4715 (1991).
[6] M. Maroncelli, J. Chem. Phys. **94**, 2084 (1991); B. M. Ladanyi and R. M. Stratt, J. Phys. Chem. **99**, 2502 (1995).
[7] M. L. Horng, J. A. Gardecki, A. Papazyan, and M. Maroncelli, J. Phys. Chem. **99**, 17311 (1995); B. M. Ladanyi and M. Maroncelli, J. Chem. Phys. **109**, 3204 (1998).
[8] B. M. Luther, J. R. Kimmel, and N. E. Levinger, J. Chem. Phys. **116**, 3370 (2002).
[9] B. M. Ladanyi and B.-C. Perng, J. Phys. Chem. A **106**, 6922 (2002).
[10] S. A. Passino, Y. Nagasawa, T. Joo, and G. R. Fleming, J. Phys. Chem. A **101**, 725 (1997).
[11] P. Suppan, J. Chem. Soc., Faraday Trans. 1 **83**, 495 (1987).
[12] N. Agmon, J. Phys. Chem. A **106**, 7256 (2002).
[13] A. Chandra, Chem. Phys. Lett. **235**, 133 (1995); A. Chandra and B. Bagchi, J. Chem. Phys. **94**, 8367 (1991).
[14] T. J. F. Day and G. N. Patey, J. Chem. Phys. **106**, 2782 (1997).
[15] A. Yoshimori, T. J. F. Day, and G. N. Patey, J. Chem. Phys. **108**, 6378 (1998).
[16] J. A. Gardecki and M. Maroncelli, Chem. Phys. Lett. **301**, 571 (1999).
[17] M. S. Skaf and B. M. Ladanyi, J. Phys. Chem. **100**, 18258 (1996).
[18] A. Yoshimori, T. J. F. Day, and G. N. Patey, J. Chem. Phys. **109**, 3222 (1998).
[19] L. R. Martins, A. Tamashiro, D. Laria, and M. S. Skaf, J. Chem. Phys. **118**, 5955 (2003).
[20] M. Sakurai and A. Yoshimori, J. Chem. Phys. **122**, 104509 (2005).
[21] S. Murata and A. Yoshimori, J. Chem. Phys. **125**, 244501 (2006).
[22] F. Cichos, A. Willert, U. Rempel, and C. von Borczyskowski, J. Phys. Chem. A **101**, 8179 (1997); F. Cichos, R. Brown, U. Rempel, and C. von Borczyskowski, *ibid.* **103**, 2506 (1999).
[23] K. Nishiyama and T. Okada, J. Phys. Chem. A **102**, 9729 (1998).
[24] T. J. F. Day and G. N. Patey, J. Chem. Phys. **110**, 10937 (1999).
[25] F. M. Floris, J. M. Martínez, and J. Tomasi, J. Chem. Phys. **116**, 5460 (2002).
[26] T. Molotsky and D. Huppert, J. Phys. Chem. A **106**, 8525 (2002).
[27] K. Sahu, S. K. Mondal, D. Roy, R. Karmakar, and K. Bhattacharyya, J. Photochem. Photobiol., A **172**, 180 (2005).
[28] One obviously needs the two solvents to have different interactions with the solute in order for the solute to have a preference. However, as has been shown beautifully in Ref. 21, one also needs to have the frustration created by having *both* solvents more strongly attracted to the excited solute than they are to the ground-state solute to end up with a nontrivial dependence of the solvation dynamics on solvent composition.
[29] M. P. Allen and D. J. Tildesley, *Computer Simulation of Liquids* (Clarendon, Oxford, 1989), Chaps. 1 and 3.
[30] G. Tao and R. M. Stratt, J. Chem. Phys. **125**, 114501 (2006).
[31] Though it is not particularly germane to the current paper, it is worth mentioning that the nonultrafast part of the solvation dynamics of this model system (the portion beyond 500 fs or so) shows excellent agreement with the expected linear response behavior for both pure and mixed solvents, C. Nguyen, Ph.D. thesis, Brown University, 2010. That is, the solvation response function S(t) closely follows the equilibrium solvation-energy correlation function for the *excited-state* solute. The corresponding equilibrium correlation function for the *ground-state* solute, by contrast, differs significantly from S(t) for mixed solvents. This kind of distinction has often been called "linear response failure" in the literature (as in, for example, Ref. 9), but as noted in Ref. 30, it might be better thought of as a lack of solute independence.
[32] W. Kob and H. C. Andersen, Phys. Rev. E **51**, 4626 (1995).
[33] J. T. Hynes, in *Ultrafast Dynamics of Chemical Systems*, edited by J. D. Simon (Kluwer, Netherlands, 1994); E. A. Carter and J. T. Hynes, J. Chem. Phys. **94**, 5961 (1991).
[34] Each Monte Carlo step consisted of a sequence of N attempted moves of 0.1σ in a randomly chosen Cartesian direction for a single, randomly chosen, particle at a time. Configurations were sampled every ten such Monte Carlo steps. Since all the points in the landscape ensemble have an equal probability density (Ref. 2), no importance sampling is needed; each move is either accepted or rejected depending on whether the final state potential energy is less than or greater than the landscape energy (respectively).
[35] Paths $\mathbf{R}_i \rightarrow \mathbf{R}_f$ were optimized by the procedure described in Ref. 3. We select a randomly chosen pivot point $\mathbf{R}_1$ along the path, displace it by a small, randomly chosen vector $\delta\mathbf{R}$, and use our standard path-finding algorithm to find two separate half-paths, $\mathbf{R}_1+\delta\mathbf{R} \rightarrow \mathbf{R}_i$ and $\mathbf{R}_1+\delta\mathbf{R} \rightarrow \mathbf{R}_f$. If the resulting combined path ($\mathbf{R}_i \rightarrow \mathbf{R}_1+\delta\mathbf{R} \rightarrow \mathbf{R}_f$) is shorter than the original path, the original path is replaced by the new, combined path. Otherwise the original path is retained. In either case, the process of trying to find shorter paths is repeated using randomly chosen pivot points along the current best path, $\mathbf{R}_2, \mathbf{R}_3, \cdots$, to generate candidate half-paths. Each candidate path is optimized with a total of ten such pivot points, with the displacements $\delta\mathbf{R}$ generated by repeatedly trying to move a randomly chosen single atom by 0.01σ in a randomly chosen Cartesian direction until the $\mathbf{R}$ point generated falls within the correct landscape ensemble. Trial optimizations using 20 pivot points were used to confirm that the optimization process had converged.
[36] R. A. LaViolette and F. H. Stillinger, J. Chem. Phys. **85**, 6027 (1986).
[37] D. Weaire and A. R. Williams, J. Phys. C **9**, L461 (1976).
[38] D. Laria and M. S. Skaf, J. Chem. Phys. **111**, 300 (1999).